Biophysical Journal Volume 71 August 1996 576–589

Small Segmental Rearrangements in the Myosin Head Can Explain Force Generation in Muscle

F. G. Díaz Baños,* J. Bordas,[#] J. Lowy,[§] and A. Svensson[¶]
*Departamento de Química Física, Universidad de Murcia, Spain; [#]Physics Department, Liverpool University, Liverpool, England; [§]Open University, Boars Hill, Oxford, England; and [¶]Physics Department, Leicester University, Leicester, England

ABSTRACT Poisson-Boltzmann calculations of the distribution of electrostatic potentials around an actin filament in physiological-strength solutions show that negative isopotential surfaces protrude into the solvent. Each protrusion follows the actin two-start helix and is located on the sites implicated in the formation of the actomyosin complex. Molecular dynamic calculations on the S1 portion of the myosin molecule indicate that in the presence of ATP the crystallographically invisible loops (comprising residues 624–649 and 564–579) remain on the surface, whereas in the absence of ATP they can move toward the actin-binding sites and experience electrostatic forces that range from 1 to 10 pN. The molecular dynamics calculations also suggest that during the ATP cycle there exist at least three states of electrostatic interactions between the loops and actin. Every time a new interaction is formed, the strain in the myosin head increases and the energy of the complex decreases by $2kT$ to $5kT$. This can explain muscular contraction in terms of a Huxley-Simmons-type mechanism, while requiring only rearrangements of small mobile S1 segments rather than the large shape changes in the myosin molecule postulated by the conventional tilting head model.

INTRODUCTION

The tilting head model has to date provided the most popular explanation for the mechanism by which force and motion are generated in contracting muscle (Huxley, 1969). Its central postulate is that contraction results from a substantial shape change in the S1 portion of myosin, which is induced by the hydrolysis of ATP. The model envisages that the myosin heads, while firmly bound to the thin filament, tilt in the direction of the muscle axis and thus produce strain. In shortening muscle this strain is relieved by the sliding motion between the thick and thin filaments. Each time the myosin heads tilt, the thin filament is propelled by a distance comparable to the length of the heads, i.e., between 10.0 and 20.0 nm (Reedy et al., 1965; Huxley, 1969; Huxley and Simmons, 1971). But in spite of intensive research over the past 25 years, there is still no unambiguous experimental evidence which proves that such large conformational changes occur in live contracting muscle.

In previous work we used time-resolved x-ray diffraction to study the structural dynamics of contracting frog muscles (Bordas et al., 1993; Martin-Fernandez et al., 1994). We argued from our results that changes in axial orientation of the heads may not be the cause of tension generation but rather the consequence of the strain imposed on them by that process. The x-ray data also indicated that although the detectable myosin heads probably adopt many different azimuthal orientations during contraction, their high degree of axial order is incompatible with random axial motions of the magnitude required by the tilting head model. Our overall conclusion was that if the detectable myosin heads performed such motions, they must be executed either by a small fraction of their total number and/or by only a small portion of their mass. According to generally accepted physiological data (Goldman and Simmons, 1977; Piazzesi and Lombardi, 1995), at least 70% of the heads are attached in isometrically contracting frog muscles. Thus, the most plausible option would appear to be that contraction involves a structural rearrangement of small mobile segments of the myosin molecule. Evidence that such motions occur is provided by NMR (Levine et al., 1990). Furthermore, studies using in vitro motility assays have shown that modifications of the myosin polypeptide chain in the region comprising the S1 flexible residues have pronounced effects in contraction (Spudich, 1994).

Because the atomic structures of the actin monomer (Kabsch et al., 1990), of the actin filament or F-actin (Holmes et al., 1990; Lorenz et al., 1993), and of S1 (Rayment et al., 1993b) are available, it is now possible to investigate by molecular dynamics calculations whether segmental rearrangements may be part of the ATP cycle and to explore how such motions may relate to various theories of contraction (Huxley and Simmons, 1971; Mitsui and Ohshima, 1993; Piazzesi and Lombardi, 1995). The results we report here constitute a first effort in this direction.

To investigate whether muscular contraction can be explained on the basis of relatively small segmental rearrangements in the motor proteins, the first step is to identify which segments take part in the formation of the actomyosin complex, and the next step is to determine the nature of the interactions involved. Fortunately, much is now known about the sites of interaction between F-actin and S1. This information may be summarized as follows.

Actin has a major site of interaction in the N-terminal region of actin at residues 1–4. These residues, which are

Received for publication 18 August 1995 and in final form 8 April 1996.

Address reprint requests to Dr. Joan Bordas, Department of Physics, Oliver Lodge Laboratory, Oxford St., Liverpool L69 38X, England. Tel.: 44-794-3361; Fax: 44-794-3441; E-mail: indx@bio.ph.liv.ac.uk.

0006-3495/96/08/576/14 $2.00

negatively charged, play a critical role in the activation of the myosin ATPase. Changes in the charges in this region have a significant influence on the maximum velocity of shortening that is reduced or increased when the number of negative charges is changed to less or more than that of native actin (Mejean et al., 1987; Miller et al., 1987; Das Gupta and Reisler, 1989, 1991; Bertrand et al., 1989; Moir et al., 1987; Van Eyk and Hodges, 1991; Sutoh et al., 1991; Aspenström and Karlsson, 1991; Cook et al., 1992, 1993). Actin has a second site of interaction in the segment 19–28, which contains the negatively charged actin residues 24 and 25. These residues are not necessary for rigor binding, but they are important for actomyosin interactions in the presence of ATP. Local charge reversal at the position of actin residues 24 and 25 results in the loss of motility and a concomitant loss of ATPase activity of myosin (Kogler et al., 1991; Van Eyk and Hodges, 1991; Adams and Reisler, 1993; Johara et al., 1993). A third site of interaction contains actin residues 99–100. These negatively charged residues, which are exposed to the solvent, interact with positively charged lysine residues on S1. Charge reversal in the region of these residues reduces the in vitro motility of F-actin by a factor of 5 (Schroder et al., 1993; Johara et al., 1993). In summary, the negatively charged regions at the N-terminal of actin and those at residues 24–25 and 99–100 are involved in myosin-driven F-actin sliding and possibly in force generation.

It is likely that each myosin head interacts with two actin monomers (Amos et al., 1982; Andreev and Borejdo, 1991; Bonafe and Chaussepied, 1995). Regarding the S1 sites implicated at the actomyosin interface, the positively charged, lysine-rich sequence spanning residues 626 and 647 at the junction of the 50K and 20K fragments (Rayment et al., 1993b) interact with the N-terminal of actin (Das Gupta and Reisler, 1989; Chaussepied and Morales, 1988; Chaussepied, 1989; Bertrand et al., 1989; Yamamoto, 1989; Rayment et al., 1993a). Furthermore, the portion of S1 between Lys-567 and His-578, which forms a highly flexible loop exposed to the solvent, is involved in binding with the negatively charged actin loops comprising residues 91–100 (Schroder et al., 1993). In addition, it has been proposed that through the positively charged lysine residues 572 and 574 this portion of the S1 interacts with the actin monomer residues 1–28 (Bonafe and Chaussepied, 1995). Dan-Moor and Muhlrad (1991) have also implicated S1 residues 143 to 147, which form a small loop on the surface of S1. Within this sequence there are four positively charged residues that show ionic strength-dependent binding.

Taken together, these observations suggest that the formation of an actomyosin complex involves actin and myosin residues with opposite charges as well as highly flexible loops in the S1 portion of the myosin molecule. This indicates that such interactions will have a substantial electrostatic component and, moreover, that the conformation of the flexible loops may play an important role in modulating F-actin and myosin head interaction.

There is also a stereospecific hydrophobic interaction in the rigor state (Schoder et al., 1993; Rayment et al., 1993a) that involves the actin hydrophobic residues Ala 144, Ile 341, Ile 345, Leu 349, and Phe 352 and the myosin residues Pro 529, Met 530, Ile 535, Met 541, Phe 542, and Pro 543. Finally, it should be noted that the S1 ATP binding site is not directly involved in the actomyosin interface, but it is in fact located on the opposite side of the myosin head. In common with Ras protein and adenylate kinase, the β-phosphate binds to the glycine-rich ATP binding sequence spanning residues 178–185 (Pai et al., 1990; Tong et al., 1991; Muller and Schultz, 1992; Rayment et al., 1993b; Gerstein et al., 1993).

In the work described in this paper, we have used molecular dynamics calculations to evaluate the mobility and conformation of the charged regions in S1 involving residues 626–647 and 572–574, which are implicated in the actomyosin interaction. We have also made calculations that show 1) the distribution of electrostatic potentials on the actin filament and on S1; 2) how in the latter the potential may be affected by the presence or absence of nucleotide; and 3) how the total energy of the actomyosin complex is affected by the various electrostatic interactions that may occur. From these calculations one can imagine a mechanism of muscular contraction based on electrostatic interactions and structural rearrangement of small mobile segments of the myosin molecule coupled to ATP hydrolysis. Such a mechanism does not require that the myosin heads undergo the large shape change postulated by the tilting head model.

METHODS

The Poisson-Boltzman equation

The spatial distribution of electrostatic potential $\phi(r)$ created by an object with an interior charge density $\rho(r)_{\mathrm{int}}$ surrounded by a medium with charge density $\rho(r)_{\mathrm{ext}}$ is given by Poisson's equation:

$$\Delta[\epsilon(r)\Delta\phi(r)] + \rho(r)_{\mathrm{int}} + \rho(r)_{\mathrm{ext}} = 0,$$

where Δ and $\epsilon(r)$ are the vector differential operator and the dielectric constant, respectively.

The Boltzman equation can be used to define the charge distribution in a solution with a given ionic strength I as

$$\rho(r)_{\mathrm{ext}} = \frac{-8\pi e^2 N_{\mathrm{A}} I}{1000kT}\,\phi(r)\left[1 + \frac{\phi(r)^2}{6} + \frac{\phi(r)^4}{120} + \ldots\right],$$

where N_{A} is Avogadro's number, e is the electron charge, k is Boltzman's constant, and T is the absolute temperature.

Introducing the Boltzman expression for $\rho(r)_{\mathrm{ext}}$ into the Poisson equation yields the so-called Poisson-Boltzman equation, i.e.,

$$\Delta[\epsilon(r)\Delta\phi(r)] + \rho(r)_{\mathrm{int}} = \frac{8\pi e^2 N_{\mathrm{A}} I}{1000kT}\,\phi(r)\left[1 + \frac{\phi(r)^2}{6} + \frac{\phi(r)^4}{120} + \ldots\right].$$

Through the construction of a solvent-accessible surface around a molecule in solution, it is possible to specify the ionic strength in the medium, the dielectric constant of the solvent, and that of the molecule.

The Poisson-Boltzman equation can then be used to calculate the distribution of electrostatic potentials.

In general, the Poisson-Boltzman equation can only be solved numerically (see, for example, Honig and Nicholls, 1995), and to this end we used the module Delphi of the Insight II package (version 2.1.0; Biosym Technologies, San Diego, Ca). This module uses a finite difference method to solve the nonlinear Poisson-Boltzmann equation (Klapper et al., 1986; Gilson and Honig, 1987). The molecule is mapped onto a three-dimensional cubic grid of specified resolution, throughout which the Poisson-Boltzmann equation is satisfied at each grid point. At each location the calculation yields the electrostatic potential due to the sum of the interaction of its charge with its own reaction field and the reaction fields of the other charges, which include those in the solvent.

The total electrostatic energy of a system can be calculated from the solution of the Poisson-Boltzman equation by the expression

$$E = \frac{1}{2} \sum_{j} q_j \phi_j,$$

where q_j and ϕ_j are the charge and the potential at the j location, and the sum runs over all locations. It follows from the above expression that to obtain a valid absolute value for E, the boundaries of the grid ought to be placed at infinity relative to the outer surface of the molecule without reducing the resolution of the grid, i.e., that of the structure. In practice this is not possible, because of computational limitations, and therefore, the absolute value obtained for the electrostatic energy of the system is dependent on the particular grid mapping employed. However, relative changes in total energy obtained from different calculations in which the same grid mapping is employed yield a valid absolute quantity. This fact was exploited in the calculations we describe below to determine the relative changes in total energy arising from different configurations of amino acid segments in the S1 molecule.

Molecular dynamics calculations

Molecular dynamics calculations aim at solving the equations of motion for a system of atoms under the influence of a force field or potential V. Newton's equation of motion relates the force field V to the motions of an atom i, at position r_i and with mass m_i, as

$$\frac{dV}{dr_i} = -m_i \frac{d^2 r_i}{dt^2}.$$

The force field V must include all terms describing the bond part of the potential energy surface, as well as nonbonding interactions between atoms, such as Lennard-Jones and electrostatic potentials. The bonding components of the force field reflect the energy needed to stretch, bend, and rotate interatomic bonds. The force field must also include components to account for cross-effects between the main bond interactions. Regarding the bond and Lennard-Jones force fields, we used the parameterized expressions that are provided within the module Discover (version 2.9) from the package Insight II. The coulombic component of the force field was defined using the dielectric constants derived with the procedures described below.

Newton's equations of motion were solved with the module Discover. This module uses the integration algorithm first described by Verlet (1967), which relies on the time interval in each integrating step to be sufficiently small to assume that the position, velocity, and acceleration of any of the atoms vary linearly. At the end of the calculation for a given time step, the velocities are updated to the new values and the process is repeated. To ensure the validity of Verlet's approximation we used time steps of 1 fs. Calculations were carried out choosing a constant pressure of 1 atm and a temperature of 300 K. This temperature was used to determine an initial set of velocities, the average of which satisfied the Maxwell-Boltzman relationship between temperature and molecular velocities.

Incorporation of the crystallographically invisible loops into the S1 structure

The positively charged sites in S1 comprising residues 626–647 and 572–574 (which we shall call the principal and minor loops, i.e., P and M loops, respectively) are highly flexible and therefore not visible in the crystallographic structure of Rayment et al. (1993b). As we wished to evaluate the effects that different nucleotide states may have on the configuration of P and M loops, it was necessary to build these loops into the S1 structure. To this end, we took the atomic positions of the α-C atoms in the S1 structure, which are available from the Brookhaven data base, and arbitrarily incorporated the absent flexible loops using the primary amino acid sequence determined for chicken pectoralis muscle by Maita et al. (1987). We argue that because of their flexibility, these loops are able to adopt many different conformations with only a small change in the total energy and that, therefore, the risk of biasing our results by the choice of the initial configuration is insignificant. We confirmed this by showing that the choice of initial configurations has no noticeable effects on the final results obtained from the molecular dynamics calculations.

Calculation of electrostatic potential surfaces on S1 and on the actin filament

The electrostatic potentials generated in solution by S1 and the actin filament were calculated by solving the Poisson-Boltzman equation. In these calculations a cubic grid with a resolution of 0.17 nm was constructed and centered on S1 and on the actin filaments in a manner such that the boundaries of the grid were located at a minimum distance of 2.0 nm beyond the furthest extent of the structures. The potential at each grid point on the boundary was determined by applying Coulomb's law separately to each charge in the structures and assuming that the only screening arises from the external dielectric constant of water. This approximation is valid, provided the molecules are sufficiently far from the boundary. Increasing the extent of the grid had no effect on the local potential calculated around the actin monomer.

The solvent region around the molecules was defined as lying between the boundaries of the grid and the solvent-accessible surface. This surface was created by rolling a sphere of specified radius around the van der Waals surface of the structure. The radius of the sphere was chosen to be equivalent to that of a water molecule, i.e., 0.18 nm. Any interstitial regions within the molecule that could not be reached by the sphere were defined as solute. The ionic strength of the solvent was set to 0.1 Mdm^{-3}. An average ionic radius of 0.2 nm was used to create a Stern layer around the solvent-accessible surface, within which the dielectric constant of water was applied while the ionic strength was set to zero.

The solute was defined as all those points of the grid that fall inside the solvent-accessible surface of the molecules. Each residue was assigned its net charge, which was placed on the appropriate atoms of the residue. Van der Waal's radii were given to each atom, with the exception of hydrogen, the radius of which was set to zero. Dielectric constants of 2 and 80 were used, respectively, for the molecules and the surrounding solvent so as to account for their electronic polarizability.

Calculation of an effective dielectric constant

To apply molecular dynamics calculations to a physiological situation it is essential to use an appropriate dielectric constant and to include the effects of electrostatic shielding due to ionic strength. To accomplish this while making the calculations practical from a computational viewpoint, we defined an effective dielectric constant ϵ_e, which simultaneously accounted for dielectric polarizability and ionic strength shielding.

To obtain a realistic estimate of ϵ_e, the following procedures were used. An assembly was constructed that consists of the whole of S1, and the P and M loops were placed at various positions relative to the rest of the molecule. Also included were the charged actin segments 1-ASP, 2-GLU, 3-ASP, 4-GLU, 5-THR, 6-THR (i.e., the six residues at the N-terminal of actin), and 97-ALA, 98-PRO, 99-GLU, 100-GLU, 101-HIS, and 102-PRO. The relative positions of these two actin segments were as defined in the structure of F-actin by Holmes et al. (1990) and Lorenz et al. (1993).

The values of the electrostatic potential at the position of the surrounding atoms were calculated before and after modifying the charge at one reference atom by adding a proton. From the difference in the potentials calculated before and after the charge was changed ($\Delta\phi$), it is possible to obtain the dielectric constant (ϵ_{ij}) operating in the electrostatic interaction between each pair of charged atoms separated by a distance r_{ij} by applying the straightforward formula for the electrostatic potential:

$$\epsilon_{ij} = \frac{\Delta q}{4\pi r_{ij}\Delta\phi}.$$

The ϵ_e used in the calculations for each loop was obtained from the distance-weighted average of the effective dielectric constant found at each of its charged atoms. For each loop we reckoned that three ϵ_e operate: 1) that in the interaction of the loop with the actin residues; 2) that in the interaction with the other loop; and 3) that with the nucleotide. During the progression of the molecular dynamics calculations, the ϵ_e used at any time was that corresponding to the longest distance from the actin for any intermediate position of the loops. This was done to produce an overestimate of ϵ_e or, in other words, an underestimate of electrostatic interactions.

To define ϵ_e we considered two different situations: when the loops were on the surface of S1, and when the loops were away from it. The values of ϵ_e obtained with these procedures for a variety of distances and loop configurations are given in Table 1. When comparisons are possible, it turns out that the values obtained are similar to those experimentally determined or calculated for other proteins (Sternberg et al., 1987; Rogers et al., 1985).

TABLE 1 Values for the effective dielectric constant calculated for various different situations and distances from the loops to the actin segments

		Ionic strength (Mdm^{-3})	Distance (nm)	Dielectric constant (ϵ_e)
ϵ_e between loops				
A		0.0	3.972	53.0
A		0.1	3.972	161.8
B		0.0	5.928	82.5
B		0.1	5.928	>1000
ϵ_e between loops and nucleotide				
A	P loop	0.0	2.266	19.5
A	M loop	0.0	1.938	23.0
A	P loop	0.1	2.266	26.5
A	M loop	0.1	1.938	37.8
B	P loop	0.0	3.686	56.9
B	M loop	0.0	3.370	67.3
B	P loop	0.1	3.686	208.5
B	M loop	0.1	3.370	655.8
ϵ_e between loops and actin				
A	P loop	0.0	3.320	66.3
A	M loop	0.0	3.002	57.9
A	P loop	0.1	1.554	147.8
A	M loop	0.1	1.366	143.5
A	P loop	0.1	2.246	427.5
A	M loop	0.1	2.584	821.9
B	P loop	0.0	2.571	67.6
B	M loop	0.0	2.195	61.0
B	P loop	0.1	1.304	47.7
B	M loop	0.1	0.976	106.7
B	P loop	0.1	1.366	265.7
B	M loop	0.1	1.204	134.4

A denotes that the loops are on the surface of S1 and B that they project away from it.

Molecular dynamics calculations on S1

Because the required computational power is not available, we could not carry out such calculations using the whole of S1 in solution. We therefore restricted the calculations to the motions of the P and M loops. So, even though for the purpose of evaluating ϵ_e we used the whole molecule, for the molecular dynamics calculations we had to define a bounded region in space that enclosed the S1 without the loops. This provided a surface through which the loops could not penetrate and, furthermore, the means to calculate the influence of S1 minus the loops on ϵ_e.

Implicit in the above procedure is the assumption that motions in the interior of the molecule, which are almost certain to occur in practice (but which cannot be calculated at present), have minor effects on the behavior of the flexible loops. Intuitively, this can be justified by the fact that because the P and M loops are either protruding from or are on the surface of S1, any internal changes will have only second-order effects on their conformation. It is also implicit in our procedure that the overall shape of S1 does not change. This has been checked over 100 ps, in vacuum and without nucleotide, by molecular dynamics calculations in which we included the first 780 residues, i.e., the globular part of S1 (Lopez Cascales et al., unpublished results).

It should be noted that as defined here, the residues in the M loop include a significant part of the segments visible in the crystallographic structure. However, because the invisible residues (572–574) are in the center of a very clear U-shaped loop that is situated on the surface of the molecule and positively unbalanced by 3.5 positive charges, it appears from the calculations that the whole of the M loop is capable of motion.

The presence of actin in the environment of S1 was accounted for by placing the segment comprising the six residues at the N-terminal, i.e., 1-ASP, 2-GLU, 3-ASP, 4-GLU, 5-THR, and 6-THR, and that including 97-ALA, 98-PRO, 99-GLU, 100-GLU, 101-HIS, and 102-PRO in their relative position as determined by crystallography. These segments provide a total of 5.5 excess negative charges on the surface of actin. In the molecular dynamics calculations, the P and M loops, the six residues at the N-terminal of actin, and the segments 97–102 of actin were allowed to move, whereas the α-carbons at the end of the segments were kept anchored at the positions specified by the atomic structure of S1 and F-actin, respectively.

In the calculations where the nucleotide, either ATP-Mg^{2+} (ATP) or ADP-Mg^{+2} (ADP), was included, it was placed in the vicinity of residues 178–185 following the method of Rayment et al. (1993a). At pH 7, both nucleotides are highly charged (Darnell et al., 1986), so the overall excess charge of ADP is expected to be -0.5 after the phosphate split. We have also assumed that the excess charge of ATP is -1.5. The position of the nucleotides was fixed during the calculations. In the case where the ADP·P_i-Mg^{+2} complex was included, we have assumed that the charge results from the addition of that of the ADP complex and that of the inorganic phosphate (-2). In this case we allowed the P_i to move freely during the calculations while the position of the ADP was kept fixed. The interior dielectric constant is different from that in the solvent (see Table 1), but as it was impossible to use different dielectric constants in different regions during the calculations, we compensated for the fact that the dielectric constant in the interior was much smaller than the one we used in the calculations by scaling the charge placed in the nucleotide.

To reduce the computational requirements, we did not include in the calculations either the flexible loop comprising residues 204 to 216, or the loop containing residues 143–147, even though both are on the surface of S1. It should be noted that although the 204–216 loop may tune the rate constant of nucleotide exchange (Spudich, 1994), and is very likely to undertake motions, it is not involved in the actomyosin interaction. Because the 143–147 loop is clearly visible in the crystal structure, its flexibility is not likely to be as high as that of the P and M loops. However, it should be noted that as this loop contains four positive charges, the expected reduction in overall energy resulting from its interaction with negatively charged regions in actin should be similar to that arising from the interaction of the P and M loops.

As pointed out above, a variety of different initial conformations were tried out, but in all cases the mean distance between the charged atoms in the loops and those in the actin residues was restricted to either 1.5 or 2.5 nm. The values we used for ϵ_e were, respectively, 150 for the first mean distance and 350 or 450 for the second mean distance (see Table 1, which shows that these values are in the required range). When the mean distance between the loops and actin was 1.5 nm, we neglected the effect of repulsion between the two loops because 1) in this situation the distance between the loops is larger than that between the loops and the actin charges; and 2) because the dielectric constant operating between the loops is much higher than that in the interactions between nucleotide loops and actin loops. In the situation where the distance between the loops and actin was 2.5 nm and $\epsilon_e = 350$, the contribution of the repulsion between loops relative to the effect due to the presence of the nucleotide was overestimated, whereas it is the other way around for $\epsilon_e = 450$.

All molecular dynamics calculations were divided into two stages. Depending on the distances between the loops and the surface of S1, we used in the first stage the criteria described above for choosing the value of ϵ_e. As the calculations proceeded, the loops moved toward the actin charges. At this point a second stage in the calculations was performed, using the smaller values for the dielectric constant which operate in these conditions (see data shown in Table 1). Typically, the time span of the first stage was 15–50 ps, whereas that of the second was extended to 40–90 ps.

RESULTS

Molecular dynamics calculations

We consider two important aspects that arise from the molecular dynamics calculations: the motions undergone by the P and M loops and the changes in energy accompanying these motions. Our results show that the behavior of the system is distinctively different, depending on which of the following situations is involved: 1) S1 with or without nucleotide and in the absence of the actin residues; 2) S1 without nucleotide and in the presence of the actin residues; 3) S1-ATP in the presence of the actin residues; and 4) S1-ADP·P_i in the presence of the actin residues. Here we illustrate typical responses of the P and M loops in each one of these four situations. Table 2 gives the initial configurations of the loops used in these examples.

S1 with or without nucleotide and in the absence of the actin residues

While going through a number of conformations, the P and M loops did not display any tendency to adopt a preferred orientation (data not shown). The changes of energy merely showed small fluctuations around the starting value. This simply confirms that in the isolated S1 molecule the P and M loops are highly mobile and disordered.

S1 without nucleotide and in the presence of the actin residues

For all of the initial configurations there were two common features in the time evolution of the system: 1) the mobility of the P loop was always greater than that of the M loop, as evidenced by the fact that the former goes through a greater number of conformations, whereas the latter tends to maintain its U shape; and 2) the final disposition of both loops was always approximately perpendicular to the surface of S1 and extended toward the actin charges (Fig. 1). We define this final configuration as the "on" state. However, the details of the evolution in the conformation of the P and M loops and in electrostatic energy of the system were found to be dependent on the initial configuration of the loops. Figs. 2 and 3 provide examples that illustrate this behavior for mean distances between the P and M loops of 2.5 and 1.5 nm, respectively.

In Fig. 2 (A traces) the loops move toward actin in a nearly monotonic fashion, although movement fluctuations and changes in electrostatic energy occur as the bond potentials exert their influence on the motion. After ~45 ps the loops have reached their "on" conformation, and the total electrostatic energy of the system at this point has been reduced by $\sim -2kT$.

In Fig. 2 (B traces) the loops move toward actin and adopt their fully extended "on" configuration in about 15 ps. At the same time, the electrostatic energy of the system drops by $\sim -3.5kT$. The time taken by the loops to reach out toward the actin residues is now much shorter than in A. This is due to the more favourable initial configuration chosen here. It should be noted that the loops continue to move and adopt a variety of configurations after reaching their "on" state, and that subsequently the electrostatic energy shows a transient increase of $\sim 2kT$ that peaks at ~25 ps while the loops move fractionally away from actin. In fact, for this particular case, the transient increase in electrostatic energy is due to the increase in bond strain arising from the fast initial motion of the loops toward actin. The trend is then reversed, and as this strain is released there is an overall reduction in the bond energy that compensates for the transient increase in electrostatic energy. Thereafter at ~45 ps, the electrostatic energy and the distance reduce and then settle at, respectively, $\sim -2kT$ and 1.5 nm, while the loops remain in their "on" configuration.

For both the A and B examples in Fig. 3 we find that the P loop reaches out toward actin and adopts the "on" configuration in about 8 ps, while the energy drops by $\sim 2kT$. In the case of B, due to a more favorable initial configuration, the M loop also adopts an "on" conformation in less than 10 ps, whereas the M loop in A takes ~25 ps to do so. Once the "on" configuration has been reached, the loops undergo a number of conformational changes, during which the electrostatic energy of the system fluctuates in response to the changes induced by the motions on the bond strain energy. After about 45 ps the system settles in the "on" configuration for both loops, and this is associated with a drop in electrostatic energy of -5 to $-6kT$. Here the much faster response of the system relative to the examples shown in Fig. 2 is due to the lower dielectric constant, as well as the initially closer position of the loops to the charged actin residues. In other examples (not shown) the drop in energy was found to be as large as $10kT$.

It should be noted that similar behavior of the loops was observed in the case of S1-ADP, but the time needed

TABLE 2 Cartesian coordinates (in nm) of the initial positions of the charged actin and myosin residues used for the calculations of the traces shown in Figs. 2, 3, and 4

Residue							
Coordinates of residues whose positions are fixed during the calculations							
		Actin				ATP (Fig. 4)	
6	0.0	0.0	0.0	α-P	−1.37	4.053	1.629
97	−0.658	0.004	0.686	β-P	−1.265	3.805	1.689
102	−0.575	−0.347	−0.393	γ-P	−1.478	3.619	1.696
6	−2.033	0.206	5.494				
97	−2.605	−0.067	6.140				
102	−2.487	−0.427	5.111				
		Myosin (Fig. 3)				Myosin (Figs. 2 and 4)	
565	−1.86	0.699	0.523		−1.129	1.944	0.662
580	−1.524	1.232	0.582		−0.843	2.496	0.704
624	−1.557	1.347	4.508		−0.999	2.322	4.621
649	−1.387	0.974	3.202		−0.775	2.051	3.297
Initial coordinates of myosin residues allowed to move during the calculations							
		Fig. 2, example A				Fig. 2, example B	
567	−1.564	2.157	−0.093		0.009	2.340	0.177
569	−2.483	3.068	0.537		−0.971	3.419	0.199
572	−2.754	3.611	−0.899		−0.692	3.682	1.331
574	0.528	2.958	0.185		−1.866	2.336	−0.606
636	−1.918	3.602	5.715		−2.900	3.472	4.855
637	−2.468	4.121	4.643		−3.173	2.636	5.910
640	−1.575	2.848	5.095		−2.124	1.945	4.371
641	−1.327	3.401	4.057		−1.920	2.536	4.438
642	−2.528	2.815	4.065		−1.908	2.783	3.847
		Fig. 3, example A				Fig. 3, example B	
567	−2.615	0.380	0.389		−0.686	1.007	0.053
569	−3.290	1.653	0.322		−1.611	2.123	0.018
572	−3.413	2.596	−0.556		−1.285	2.455	1.120
574	−2.968	1.299	−0.782		−0.432	1.600	0.098
636	−3.140	2.520	5.089		−3.396	2.600	4.708
637	−3.822	1.413	5.527		−3.674	1.854	5.826
640	−2.529	1.047	4.074		−2.705	1.005	4.315
641	−2.406	1.811	4.224		−2.471	1.592	4.334
642	−2.657	1.799	3.500		−2.476	1.794	3.726
		Fig. 4, example A				Fig. 4, example B	
567	−0.001	1.820	0.186		−1.564	2.157	−0.093
569	−0.958	2.919	0.095		−2.483	3.068	0.537
572	−0.090	4.342	0.603		−2.754	3.611	−0.899
574	−1.866	2.336	−0.606		0.228	2.943	0.276
636	−2.956	3.409	4.860		−1.918	3.602	5.715
637	−3.345	2.634	5.697		−2.468	4.121	4.643
640	−2.074	1.891	4.346		−1.575	2.848	5.095
641	−1.911	2.560	4.485		−1.327	3.401	4.057
642	−1.937	2.878	3.848		−2.528	2.815	4.065

The labels on the columns of coordinates indicate to which set of calculations the coordinates correspond. For the spatially fixed residues, the positions are given by the coordinates of their α-carbon. When used, the position of ATP is given by the coordinates of the phosphorous atoms in the α, β, and γ phosphate. The initial positions of the residues allowed to move are defined by the coordinates of the nitrogen atoms in the amino terminal.

to open the loops was longer and the overall reduction in electrostatic energy was, on average, smaller.

In summary, the calculations show that in nucleotide-free S1, and in the presence of actin residues, the loops move away from the surface of S1 toward actin and adopt the "on" configuration. In doing so, the positively charged residues move by 1.0–2.0 nm and, depending on the initial distance between the loops and actin, and when the loops reach the "on" configuration, the electrostatic energy of the system can decrease by anything between 2 and 10 kT. The times for the loops to reach this configuration can be as fast as 7–10 ps for the shorter initial mean distance of 1.5 nm between actin and the position of the loops, and as slow as 40–60 ps for the longer distance of 2.5 nm and for unfavorable initial configurations.

S1-ATP in the presence of the actin residues

The calculations show that in the presence of ATP the loops tend to remain close to the surface of S1. We define this configuration as the "off" state (see Fig. 1).

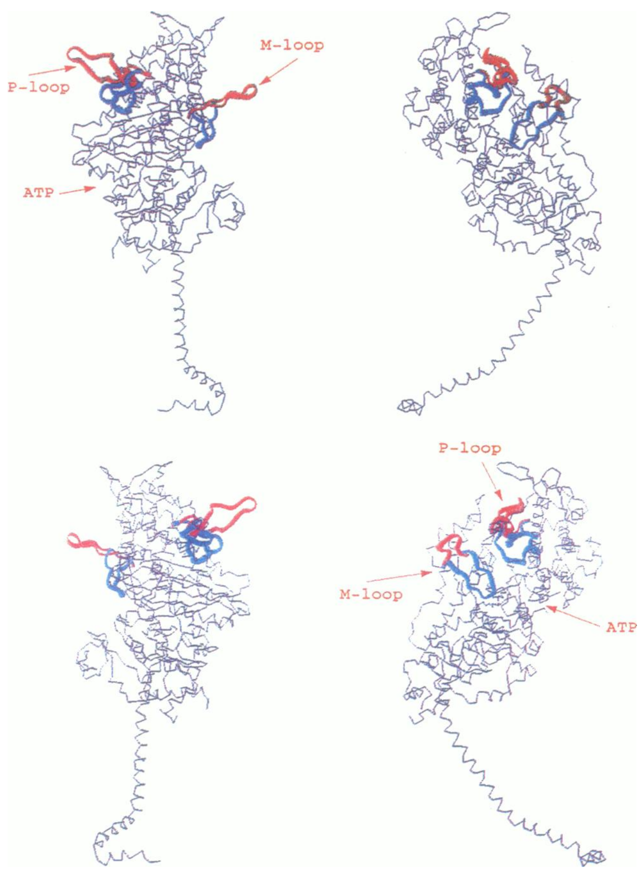

FIGURE 1 Several views of the polypeptide backbone of S1 showing the conformations that, according to molecular dynamics calculations, are adopted by the P and M loops in the presence (blue; "off" state) and in the absence (red; "on" state) of ATP (see text for definitions). Scanning the page in a clockwise direction, the view is rotated each time by 90° around a vertical axis running through the middle of S1. Note that while in the presence of ATP the P and M loops are folded over the body of S1; in the absence of ATP these loops project out almost perpendicular to the surface of S1.

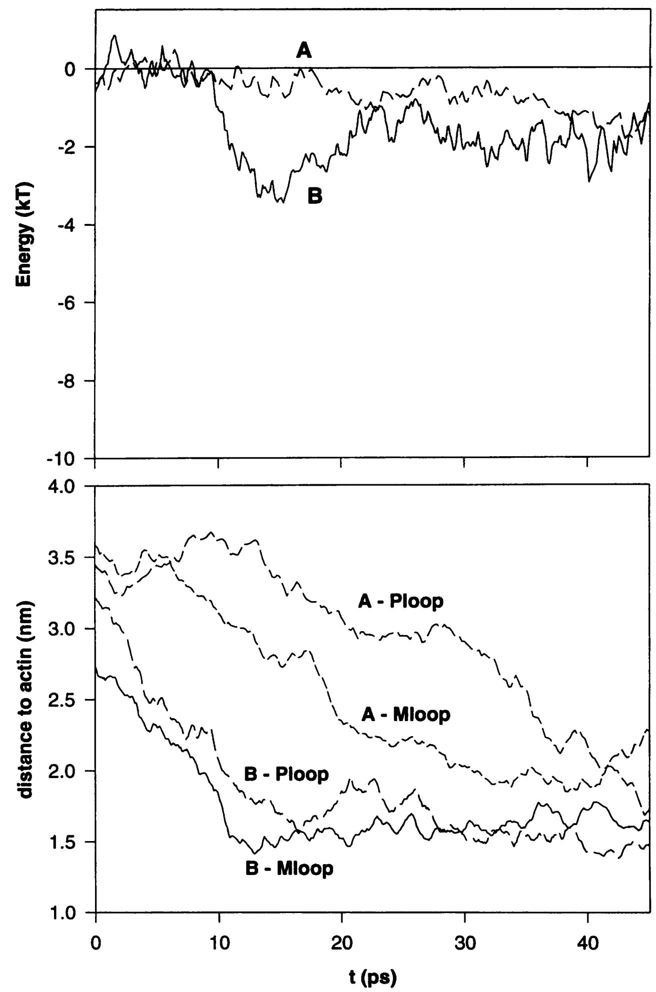

FIGURE 2 Traces illustrating the behavior of the system in the absence of nucleotide for a mean distance of 2.5 nm between the charged residues in the P and M loops and the charged actin residues. (*Top*) Evolution of the energy. (*Bottom*) Positions of the P and M loops. ϵ_e was given a value of 350 (see Table 1). Traces labeled A correspond to an initial configuration in which the loops were deliberately placed with the charged residues pointing away from actin (see Table 2 for coordinates). Traces labeled B correspond to an initial configuration in which the P and M loops were placed in an arbitrary configuration near the surface of S1 (see Table 2 for coordinates). The vertical axis in the top panel is defined as the mean distance between the nitrogen atoms in the amino terminal of the positively charged lysine residues (five lysines in the P loop and four in the M loop) and the α-carbon in the 6-THR residue of actin. The position of the α-carbon is arbitrarily chosen as the origin (see Table 2 for initial coordinates).

The loops occasionally failed to maintain the "off" state when the initial configuration of either loop included a charged residue at a distance from actin shorter than 1.0 nm. In that case, depending on the starting distance from actin, either the loops moved toward actin or remained in the vicinity of their initial position. In either case there were no significant changes in overall electrostatic energy.

When the loops did not move toward the actin charges, i.e., in all configurations where the distance of any charged residue from actin was greater than 1.0 nm, the loops moved toward the position occupied by ATP, and in some cases, if not stopped, they would have penetrated into S1. The data shown in Fig. 4 show two typical examples of this behavior for $\epsilon_e = 450$ (A traces) and $\epsilon_e = 350$ (B traces).

In the A example, the total electrostatic energy undergoes fluctuations around the starting value (Fig. 4 *a*), whereas the positively charged residues in both the P and M loops tend to drift away from actin (Fig. 4 *b*) and to get closer to ATP (Fig. 4 *c*).

In some cases the loops would eventually attempt to penetrate the surface of S1. An illustration of such a behavior is provided by the B example. Here both loops move away from actin and toward the ATP within 8 ps of initiating the sequence (Fig. 4, *b* and *c*). This is accompanied by a drop of $\sim 2kT$ in the electrostatic energy. Thereafter the M loop penetrates the surface of S1 with the consequent decrease in electrostatic energy. At this point the calculation was stopped.

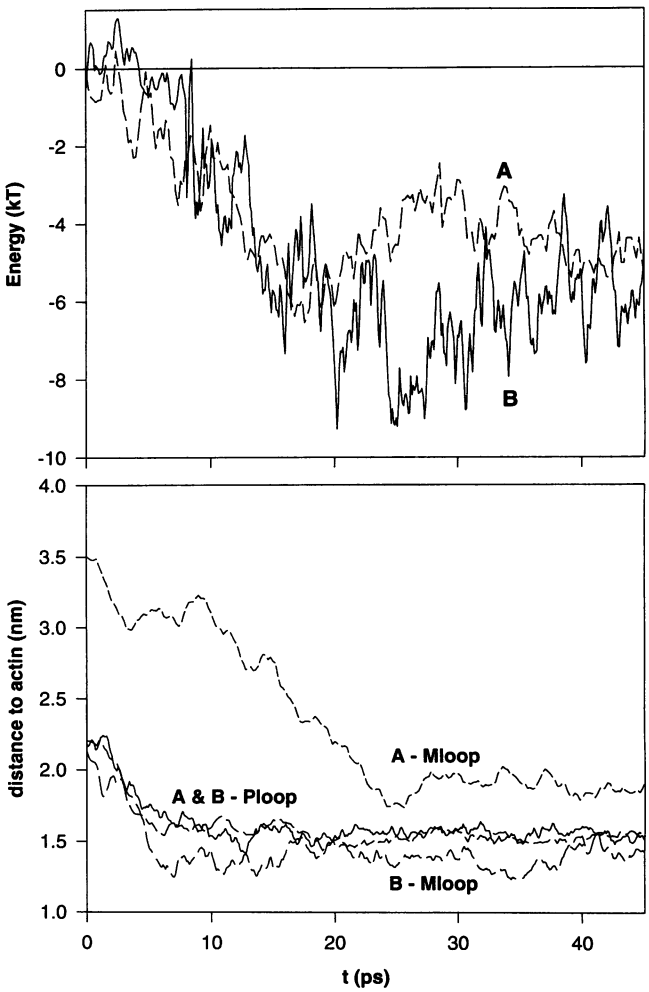

FIGURE 3 Traces illustrating the behavior of the system in the absence of nucleotide for a mean distance of 1.5 nm between the charged residues in the P and M loops and the charged actin residues. (*Top*) Evolution of the energy. (*Bottom*) Positions of the P and M loops. ϵ_e was given a value of 150 (see Table 1). Traces labeled A and B correspond to two different initial configurations of the P and M loops, the coordinates of which are given in Table 2. The vertical axis in the bottom panel is the same as that in Fig. 2, *bottom*.

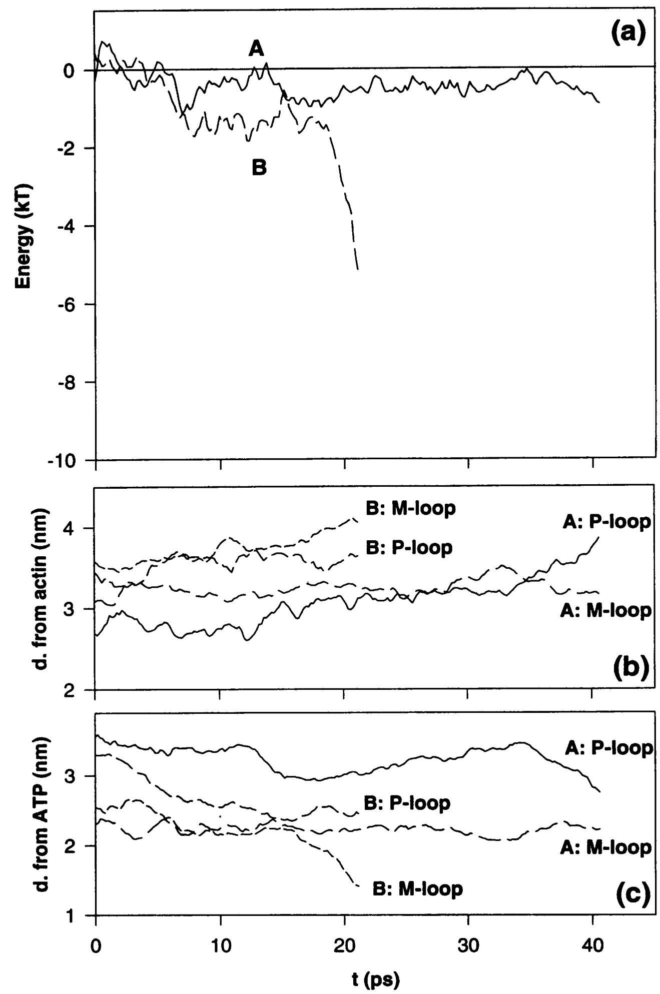

FIGURE 4 Traces illustrating the behavior of the system in the presence of ATP for a mean distance of 2.5 nm between the charged residues in the P and M loops and the charged actin residues. (*a*) Evolution of the energy in the system. (*b* and *c*) Positions of the P and M loops, respectively. The definition for the distance in *b* is the same as that in Figs. 2 (*bottom*) and 3 (*bottom*). That in *c* is the distance from the loops to an origin arbitrarily placed at the α-phosphate in the ATP molecule. The results illustrate the behavior for ϵ_e = 450 (A traces) and ϵ_e = 350 (B traces).

In summary, it appears that for S1-ATP any significant changes in electrostatic energy are due to the loops moving toward the ATP pocket (see Fig. 1) and that the electrostatic interaction between actin and S1 is either balanced or counteracted by the loops interacting with the ATP molecule.

S1 in ADP·P$_i$ and in the presence of the actin residues

Molecular dynamics calculations (not presented here) in which we studied the effect of the release of the γ-phosphate, showed that depending on the initial orientation chosen for the insertion of the nucleotide into the ATP pocket of S1, the γ-phosphate moved either toward the P loop or toward the M loop by traveling along the channel formed in the interface between the 50-kDa and 20-kDa domains. In other words, the γ-phosphate tends to leave S1 via the "back door" (Yount et al., 1995). After the P_i has reached a loop, it either stays in its surroundings and follows its movements, or it is expelled from the structure into the solvent. In fact, both types of behavior have been observed in the calculations. We note that when the γ-phosphate is ejected and only ADP is left in the S1 pocket then, as described above, both loops tend to move toward the actin charges. It should also be noted that in isolated S1-ATP one or both of the loops may cover the "back door." In that case, phosphate ejection and subsequent nucleotide exchange will more plausibly be accomplished via the "front door" (i.e., the entrance into the nucleotide pocket around residues 204–216), although possibly at slower rates because of steric impediments. This is in line with the suggestion of Yount et al. (1995), which was based on the mechanism proposed by

Gilson et al. (1994) for acetylcholine esterase, and by Hyde et al. (1988) for tryptophan synthase. However, as the actin charge "straightens" the loops, the terminal phosphate is dragged along with it and after exposure to solvent is ejected via the "back door." Spudich (1994) discussed the importance of the P loop in determining the maximum speed of shortening and speculated about its role in triggering the release of P_i.

Electrostatic potential surfaces on S1 and actin filaments

Fig. 5 shows electrostatic isopotential differences between S1-ATP and S1 at $0.5kT$ (red) and at $-0.5kT$ (blue). As expected, the most notable feature is that the S1 state has a substantially higher positive potential around the region of the "on" loops and that this potential protrudes into the solvent. These results suggest that as the loops open out and adopt the "on" conformation, the redistribution in potential allows the full development of electrostatic interaction with F-actin.

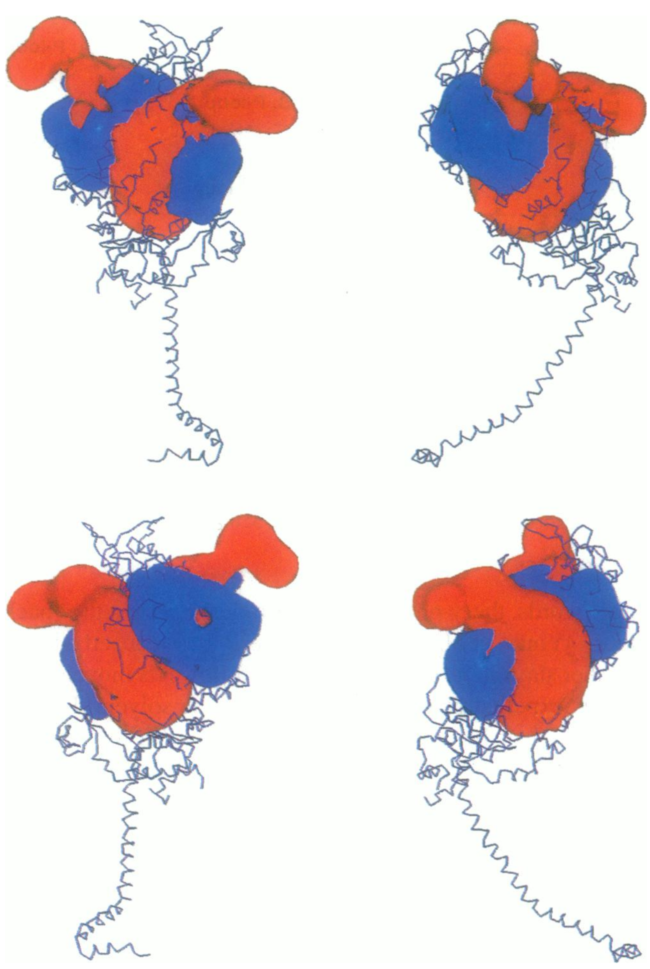

FIGURE 5 Electrostatic potential surfaces corresponding to the difference in potential between S1 and S1-ATP. The contours are shown for a potential energy difference of 0.5 kT (red) and -0.5 kT (blue). The views of S1 are the same as those in Fig. 1.

Fig. 6 shows the electrostatic potential at constant values of $+0.5kT$ and $-0.5kT$ determined for an actin filament containing 15 actin subunits. These potential surfaces are relative because they include the small constant contribution due to artefacts from the grid mapping. There is a large negative potential bulge strongly localized in the vicinity of the sites that contain the acidic residues and are involved in the formation of an actomyosin complex. This bulge in the negative potential surface extends radially out from the N-terminus by ~2 nm. It is apparent that even at this distance of 2 nm, the negative potential surface at the binding site follows the profile of the actin two-start helix.

In this connection it is appropriate to mention that there are 14 possible actin-binding sites on each molecule of tropomyosin that bind to seven actin monomers (Hitchcock-DeGregori and Varnell, 1990). Our calculations show that the distribution of positive potentials in F-actin may be important in locating the tropomyosin. We find two lines of seven positive potential lobes for every seven actin monomers (Fig. 6). One of these lines is located above the large negative potential lobe and lies approximately on the position of tropomyosin in relaxed muscle. The other line is placed almost at the center of the groove of the long-pitch helix. Thus, our calculations suggest that the reason why the thin filament does not allow an interaction with myosin heads when muscle is inactivated is because the negative potential bulge is at least partly screened by the tropomyosin molecule. One can envisage that on activation the troponin molecules undergo a conformational change induced by Ca^{2+} binding. This leads to an excess negative charge in the tropomyosin molecule, which destabilizes the interactions operating at rest between tropomyosin and F-actin. It is conceivable that as a result, tropomyosin, which has an alternating disposition of negatively and positively charged residues, moves away from the vicinity of the F-actin sites that were occupied at rest. After this motion, tropomyosin could settle in a position which coincides with that of the electropositive potential strand closer to the center of the long-pitch helix groove (see Fig. 6). This is indeed the position occupied by tropomyosin when the thin filament is in Ca^{2+} (Lehman et al., 1994; Poole et al., 1995). At this moment the actin filament is activated and the full electrostatic potential is available for interaction with S1. This kind of thin-filament activation is in agreement with the notion of a "biological ratchet," as described by Levine et al. (1990).

DISCUSSION

The calculations presented above confirm the flexibility of the P and M loops, which is expected from their high content of lysines, the dihedral angles of which can easily rotate. The calculations also show that the nucleotide-modulated electrostatic interactions we have described are only possible because both loops are flexible and can therefore

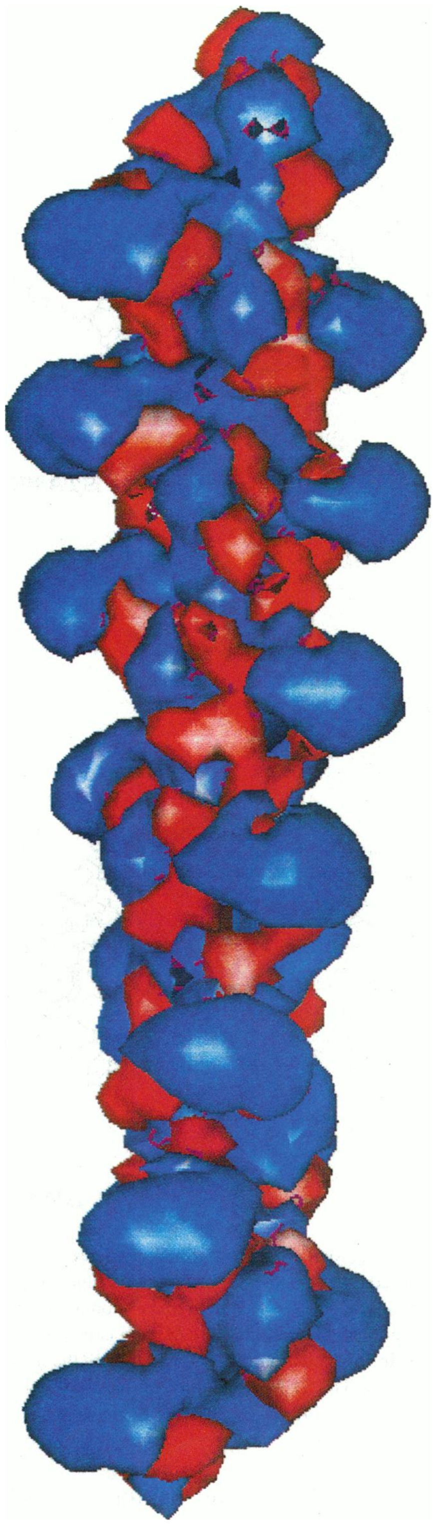

FIGURE 6 Electrostatic potential surfaces calculated for F-actin. The regions of negative potential contoured at 0.5 kT are shown in blue, and those at -0.5 kT are shown in red.

adopt the most effective configuration when interacting with the actin charges. Thus, while in the absence of the actin charges, the loops in S1 without nucleotide remain mobile, and when these actin charges are present the mobility of the S1 loops is greatly reduced. This is in line with NMR observations of the stabilization of these same loops during the interaction of S1 with actin (Levine et al., 1990). Taken together, the results suggest that electrostatic interactions only operate between actin and S1 when the latter is in the ADP or, particularly strongly, in the nucleotide-free state. Such behavior of the loops suggests a model for contraction that does not require large shape changes of the myosin heads but relies on the rearrangement of relatively small segments. This idea is further elaborated on below. Here we consider possible answers to four questions:

1. Can the electrostatic interactions we have described generate forces of a magnitude similar to those observed experimentally? The force produced at any one time between S1 and the thin filament depends on the distance between charges and the dielectric constant. Assuming that the positively charged loops are placed somewhere between 2.5 and 1.5 nm away from the actin surface, and that the dielectric constant (which includes electrostatic shielding due to ionic strength) is in the range of 150 to 450, we find that the electrostatic forces between F-actin and the P or the M loop amount to anything between 1.3 and 13 pN. These values are in the range of those experimentally determined by in vitro motility assays (Ishijima et al., 1994; Finer et al., 1994).

2. Can such electrostatic forces provide a plausible explanation for muscular contraction? A condition for explaining contraction is that the interaction between myosin and activated actin filaments should be modulated by the nucleotide state of the myosin head. That this may be so is shown by Figs. 1–4, which demonstrate that the position of the loops depends on whether S1 has bound ATP or ADP or is in a nucleotide-free state. Thus, when S1 has bound ATP, the loops are folded over its body and do not protrude into the solvent. When S1 is in the ADP state, the loops tend to extend toward actin. Finally, in the absence of nucleotide, the loops open up and project well away from the surface of S1. Evidently, the strength of electrostatic interactions is largest in the absence of nucleotide.

3. Can unidirectional motion and/or force production be generated by electrostatic interactions? The central postulate of most models put forward to explain the mechanical and energetic behavior of muscles is that there must be at least three different types of interaction between myosin heads and the thin filament, and that each of these interactions has a different potential energy well, the depth of which is greater as one moves along the direction of shortening. The probability of a head being in any of the three states is usually calculated from the construction of three potential wells with depth differences and a potential of the elastic type (Huxley and Simmons, 1971). It is also usually assumed that the elastic element is located entirely in the myosin heads. However, for the purpose of the present discussion, this element could be either in the heads or in the backbone of the myosin filament or in both. The depth differences in the potential wells are usually treated as adjustable parameters, to obtain during quick releases or

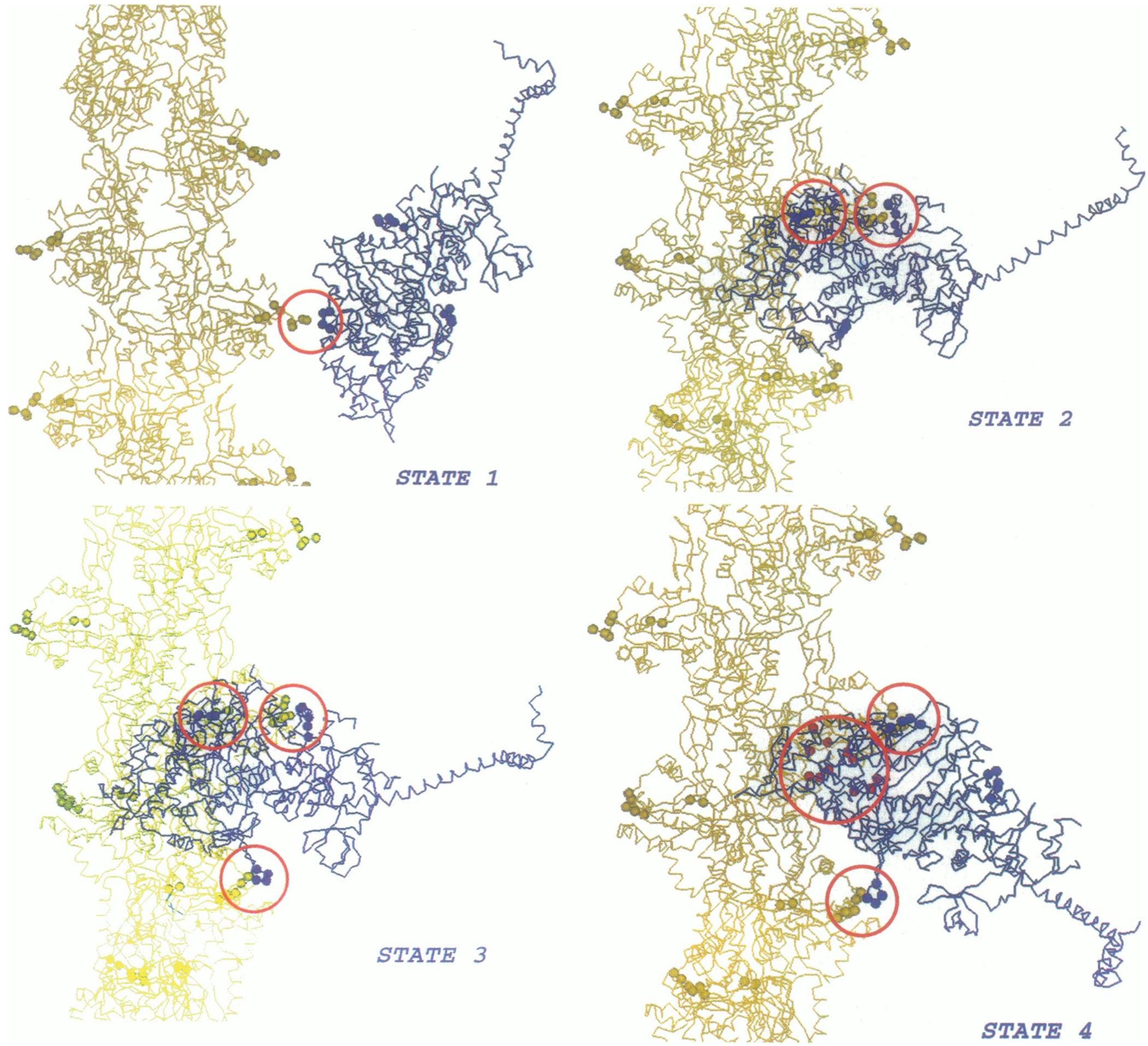

FIGURE 7 Illustration of several possible states of interaction between F-actin and S1 in which the total energy progressively decreases. The negatively charged actin segments that interact with S1 are labeled with green spheres. The positively charged S1 segments are labeled with blue spheres. The points of contact are circled in red. In state 1 the actin N-terminal makes contact with the extended P loop. In state 2, the P loop makes contact with actin residues 24–26, and S1 residues 143–147 are in touch with the actin N-terminal. In state 3 the contacts are as in state 2, but the M loop contacts residues 99–100 in the next actin monomer. State 4 depicts the interactions in rigor where the energy is lowest. In this situation the P loop contacts the actin monomer at the N-terminal, and the M loop is in contact with actin residues 99–100 in the next actin monomer. The S1 hydrophobic residues 529–543 (labeled with red spheres) are embedded in the hydrophobic pocket of actin. Here the contact involving S1 residues 143–147 cannot be made.

stretches the correct ratios of the T_2, T_3, and T_4 curves relative to the T_o curve, as well as to derive the probability of occupancy of the three states and the right kinetics of the processes (Huxley and Simmons, 1971; Piazzessi and Lombardi, 1995; Mitsui and Ohshima, 1993). Typical potential depth differences range from 2.5 to $5kT$, the exact value depending on which data are being fitted and what assumptions are made about the stiffness of the elastic element.

4. Can such potential depth differences be obtained with a force generation model based on electrostatic interactions? The following arguments show that this is readily done. S1 has three positively charged loops: the P loop, the M loop, and the 143–147 loop, with excess charges equivalent to 3, 3.5, and 4 protons, respectively. These loops are known to be involved in the interaction with actin. The minimum state of energy will be the one in which all three loops have a minimum distance to the charged actin sites, which in practice probably means that S1 makes three contacts with two actins. If a myosin head makes only two contacts with actin, then the energy of the system will be higher, and

when only one contact is made, this state will have the highest energy—excluding, of course, the case in which no contacts are made.

By way of illustration, let us consider the three states of interaction in Fig. 7. State 1 is shown with S1 and actin making only one contact, namely the P loop with the N-terminal of actin. This is the state with the highest energy. Because the other two possible contacts are not made, we find that the strain on the elastic element is minimal. As mentioned above, for present purposes, this element may be in several possible locations. One can also consider a form of interaction such as that shown in state 2. Such an interaction involves two contacts, which here are the P loop contacting residues 24–26 in the actin monomer and the S1 residues 143–147 contacting the residues on the actin N-terminal. This state will have a lower energy than state 1, but to make the contacts the elastic element will be more stretched because the S1 has to pivot to develop the new interaction. Finally, one can consider the situation with the lowest energy, such as that shown in state 3. Here three contacts are made: 1) the P loop in contact with actin residues 24–26; 2) the S1 residues 143–147 in contact with the actin N-terminal; and 3) the M loop in contact with actin residues 99–100 in the next actin monomer. Note that in state 3 the elastic element will be stretched to the greatest extent.

One can imagine several variations of the states depicted in Fig. 7, but in all cases the more contacts that are made, the lower the energy and the greater will be the stretch of the elastic element. The calculations illustrated in Figs. 2–4 reveal that every time a new contact is made, the free energy will drop by 2–10kT. This means that the requirements of the energy diagrams used in widely accepted theories of contraction, based on the hypothesis of Huxley and Simmons (1971), can easily be fitted and given a structural basis for the three states of interaction with actin. Moreover, from an energetic point of view, all variations of the scheme shown in Fig. 7 lead essentially to the same results.

A fourth state of even lower energy can be envisaged. This can occur when the S1 hydrophobic residues 529–543 are embedded in the hydrophobic pocket of actin. To effect such an interaction, it is necessary to break the electrostatic contact involving S1 residues 143–147, and (relative to the thin filament axis) the myosin head must adopt a more tilted orientation than in state 3. This configuration (state 4) is practically identical to that deduced for the rigor state by Rayment et al. (1993a). In passing, it should be noted that given their electrostatic nature, interactions of the type shown for states 1, 2, and 3 will exhibit an ionic strength dependence. On the other hand, interactions as depicted in state 4 that involve hydrophobic bonds will not be affected to the same degree by the ionicity of the medium.

In the transition from state 1 to 2 there will be both a radial and a longitudinal component to the stretch exerted on the elastic element. Because one is dealing with a three-dimensional situation in which all of the forces add vectorially, it is difficult to make an accurate estimate of the magnitude of these two components without elaborate calculations, and this is outside the scope of the present paper. Complications arise because the configuration of the initial S1 attachment in a non-tension-generating situation (i.e., a situation akin to state 1 in Fig. 7) is not known, and because the electrostatic pull at any one time will depend on the distance between the loops and the actin charges. However, assuming 1) that the angle of attachment in state 1 is similar to that adopted by the head at rest (i.e., ~45°C to a plane perpendicular to the muscle axis); 2) that in state 2 the main bulk of the myosin head is perpendicular to the muscle axis (Bordas et al., 1993); and 3) that the electrostatic pull on the M loop amounts to anything between 1.3 and 13 pN, we find that the force exerted on the elastic element has a radial and a longitudinal component in the range of 1 to 9 pN.

Irrespective of any of the considerations discussed above, our molecular dynamics calculations show that the energy of the actomyosin complex is reduced by 2–10kT every time a new electrostatic interaction is developed via contacts between the S1 loops and the charged actin sites. The magnitude of these potential differences is very similar to that required by Mitsui and Ohshima (1993) and Piazzessi and Lombardi (1995) to explain the mechanical response of muscles to quick releases and stretches.

On our model the myosin heads may have at least three orientations. The heads in states 2 and 3, which develop the most tension, will adopt a more perpendicular orientation to the muscle axis than those in state 1, which develop the least tension. It is apparent that the orientation of S1 will be more rigid the more contacts that are made. However, given the different symmetries of the myosin and the surrounding actin filaments, one would expect that on activation there will be a range of azimuthal orientations of the heads. Initially most of the heads will adopt a configuration of the type shown in state 1. As tension develops, one expects an increase in the population of heads in states 2 and 3. Regardless of the variability in azimuthal orientation, this kind of model would predict that the axial orientation of the heads will remain fairly fixed. This is in line with both x-ray diffraction (Bordas et al., 1993) and electron microscope observations (Hirose et al., 1993, 1994), which indicate that whereas a fairly high degree of axial order exists in contracting muscle, there is a substantial amount of azimuthal variability in the orientation of the myosin heads. In fact, it is only in the rigor state, which has the lowest energy, that both the azimuthal and axial orientations must be rigidly fixed.

It should be noted that interactions such as those described here can only take place if the thin filament is activated, otherwise tropomyosin prevents one of the loops (probably the P loop) from interacting with actin residues 24–26. Tropomyosin probably also has another effect in that it could sterically limit the interaction of S1 with two successive actins, as depicted in state 3. Moreover, it should be noted that according to Dan-Moor and Muhlrad (1991), interaction between S1 residues 143–147 and actin is essential for the ATPase activity of S1. This means that the hydrolysis of the nucleotide should be most prominent in states 2 and 3. These observations are in line with results which showed that actin residues 24–28 are necessary for the activation of myosin ATPase (Kogler et al., 1991; Van Eyk and Hodges, 1991).

We conclude from these several arguments that it is possible to envisage a mechanism of muscular contraction based on electrostatic interactions and structural rearrangements of small mobile segments in the myosin molecule coupled to ATP hydrolysis. Such a mechanism does not require that the myosin heads undergo the large shape changes postulated by the tilting head model. The "working stroke" in our mechanism is to be regarded as the range of interaction that can occur while S1 remains in the "on" state after a quick release.

X-ray diffraction results and deductions from experiments with live contracting frog muscles suggest that the requirements of the tilting head model can only be met if contraction involves just a small fraction of the total population of heads and/or a small portion of their mass (Martin-Fernandez et al., 1994). Our model reconciles these x-ray data with the various formulations of the Huxley-Simmons model. The small fraction of the mass would be the domain rearrangement involving the P and M loops.

We would like to thank J. Harries for his contribution to the early stages of this work and G. Diakun for helpful discussions. The provision of facilities of the Daresbury Laboratory is gratefully acknowledged.

FGDB was supported by a fellowship from the Human Capital and Mobility Programme (project ERB4050PL930014).

REFERENCES

Adams, S., and E. Reisler. 1993. Role of sequence 18–29 on actin in actomyosin interactions. *Biochemistry.* 32:5051–5056.

Amos, L. A., H. E. Huxley, K. C. Holmes, R. S. Goody, and K. A. Taylor. 1982. Structural evidence that myosin heads may interact with two sites on F-actin. *Nature.* 299:467–469.

Andreev, O. A., and J. Borejdo. 1991. The myosin head can bind two actin monomers. *Biochem. Biophys. Res. Commun.* 177:350–356.

Aspenström, P., and R. Karlsson. 1991. Interference with myosin subfragment-1 by site directed mutagenesis of actin. *Eur. J. Biochem.* 200: 35–41.

Bertrand, R., P. Chaussepied, E. Audermard, and R. Kassab. 1989. Functional characterisation of skeletal F-actin labelled on the NH_2-terminal segment of residues 1–28. *Eur. J. Biochem.* 181:747–754.

Bonafe, N., and P. Chaussepied. 1995. A single myosin head can be cross-linked to the N termini of two adjacent actin monomers. *Biophys. J.* 68:35s–43s.

Bordas, J., G. P. Diakun, F. G. Diaz, J. E. Harries, R. A. Lewis, J. Lowy, G. R. Mant, M. L. Martin-Fernandez, and E. Towns-Andrews. 1993. Two-dimensional time-resolved X-ray diffraction studies of live isometrically contracting frog sartorius muscle. *J. Muscle Res. Cell Motil.* 14:311–324.

Chaussepied, P. 1989. Interaction between stretch of residues 633–642 (actin binding-sites) and nucleotide binding-site on skeletal myosin subfragment-1 heavy-chain. *Biochemistry.* 28:9123–9128.

Chaussepied, P., and M. F. Morales. 1988. Modifying preselected sites on proteins: the stretch of residues 633–642 of the myosin heavy-chain is part of the actin-binding site. *Proc. Natl. Acad. Sci. USA.* 85:7471–7475.

Cook, R. K., W. T. Blake, and P. A. Rubenstein. 1992. Removal of the amino-terminal acidic residues of yeast actin. Studies "in vitro" and "in vivo." *J. Biol. Chem.* 267:943–9436.

Cook, R. K., D. Root, C. Miller, E. Reisler, and P. A. Rubenstein. 1993. Enhanced stimulation of myosin subfragment 1 ATPase activity by addition of negatively charged residues to the yeast actin NH_2 terminus. *J. Biol. Chem.* 268:2410–2415.

Dan-Moor, M., and A. Muhlrad. 1991. Antibody directed against the 142–148 sequence of the myosin heavy-chain interferes with myosin actin interaction. *Biochemistry.* 30:400–405.

Darnell, J., H. Lodish, and D. Baltimore. 1986. Molecular Cell Biology. Scientific American Books, New York.

Das Gupta, G., and E. Reisler. 1989. Antibody against the amino terminus of alpha-actin inhibits actomyosin interactions on the presence of ATP. *J. Mol. Biol.* 207:833–836.

Das Gupta, G., and E. Reisler. 1991. Nucleotide-induced changes in the interaction of myosin subfragment 1 with actin: detection of antibodies against the N-terminal segment of actin. *Biochemistry.* 30:9961–9966.

Finer, J. T., R. M. Simmons, and J. A. Spudich. 1994. Single myosin molecule mechanics: piconewton forces, and nanometer steps. *Nature.* 368:113–118.

Gerstein, M., G. Schulz, and C. Chothia. 1993. Domain closure in adenylate kinase-joins on either side of 2 helices close like neighbouring fingers. *J. Mol. Biol.* 229:494–501.

Gilson, M. K., and B. H. Honig. 1987. Calculation of electrostatic potentials in an enzyme active-site. *Nature.* 330:84–86.

Gilson, M. K., J. P. Strautsma, J. A. McCammon, D. R. Ripolli, C. H. Faerman, D. H. Axelsen, I. Silman, and J. L. Sussman. 1994. Open back door in a molecular-dynamics simulation of acetyl cholinesterase. *Science.* 263:1276–1278.

Goldman, Y. E., and R. M. Simmons. 1977. Active, and rigor muscle stiffness. *J. Physiol. (Lond.).* 269:55–57.

Hirose, K., C. Franzini-Armstrong, Y. E. Goldman, and J. M. Murray. 1994. Structural changes in muscle cross-bridges accompanying force generation. *J. Cell Biol.* 127:763–778.

Hirose, K., T. D. Lennart, J. M. Murray, C. Franzini-Armstrong, and Y. E. Goldman. 1993. Flash, and smash: rapid freezing of muscle fibres activated by photolysis of caged ATP. *Biophys. J.* 65:397–408.

Hitchcock-DeGregori, S. E., and T. A. Varnell. 1990. Tropomyosin has discrete actin-binding sites with 7-fold, and 14-fold periodicities. *J. Mol. Biol.* 214:885–896.

Holmes, K. C., D. Popp, W. Gebhard, and W. Kabsch. 1990. Atomic model of the actin filament. *Nature.* 347:44–49.

Honig, B., and A. Nicholls. 1995. Classical electrostatics in biology, and chemistry. *Science.* 268:1144–1149.

Huxley, A. F., and R. M. Simmons. 1971. Proposed mechanism of force generation in striated muscle. *Nature.* 233:533–538.

Huxley, H. E. 1969. The mechanism of muscular contraction. *Science.* 114:1356–1366.

Hyde, C. C., S. A. Ahmed, E. A. Padlan, E. W. Miles, and D. R. Davies. 1988. Three-dimensional structure of the tryptophan synthase α-2-β-2 multienzyme complex from *Salmonella typhimurium. J. Biol. Chem.* 263:17857–17871.

Ishijima, A., Y. Harada, H. Kojima, T. Funatsu, H. Higuchi, and T. Yanagida. 1994. Single-molecule analysis of the actomyosin motor using nano-manipulation. *Biochem. Biophys. Res. Commun.* 199: 1057–1063.

Johara, M., Y. Y. Toyoshima, A. Ishijima, H. Kojima, T. Yanagida, and K. Sutoh. 1993. Charge-reversion mutagenesis of *Dictyostelium* actin to map the surface recognised by myosin during ATP-driven sliding motion. *Proc. Natl. Acad. Sci. USA.* 90:2127–2131.

Kabsch, W., H. G. Mannherz, D. Suck, E. F. Pai, and K. C. Holmes. 1990. Atomic-structure of the actin DNase I complex. *Nature.* 347:37–44.

Klapper, I., R. Hagstrom, R. Fine, K. Sharp, and B. Honig. 1986. Focusing of electric fields in the active site of Cu-Zn superoxide dismutase: effects of ionic strength, and amino-acid modification. *Proteins.* 1:47–59.

Kogler, H., A. J. Moir, I. P. Trayer, and J. C. Ruegg. 1991. Peptide competition of actin activation of myosin subfragment-1 ATPase by an amino terminal actin fragment. *FEBS Lett.* 294:31–34.

Lehman, W., R. Craig, and P. Vibert. 1994. Ca^{2+}-induced tropomyosin movement in limus thin filament revealed by 3-dimensional reconstruction. *Nature.* 368:65–67.

Levine, B. A., A. J. G. Moir, I. P. Trayer, and R. J. P. Williams. 1990. *In* Molecular Mechanisms in Muscular Contraction. J. M. Squire, editor. 171–209.

Lorenz, M., D. Popp, and K. C. Holmes. 1993. Refinement of the F-actin model against X-ray fibre diffraction data by the use of a directed mutation algorithm. *J. Mol. Biol.* 234:826–836.

Maita, T., M. Hayashida, Y. Tanioka, Y. Komine, and G. Matsuda. 1987. The primary structure of the myosin head. *Proc. Natl. Acad. Sci. USA.* 84:416–420.

Martin-Fernandez, M. L., J. Bordas, G. P. Diakun, J. E. Harries, J. Lowy, G. R. Mant, A. Svensson, and E. Towns-Andrews. 1994. Time-resolved X-ray diffraction studies of myosin head movements in live frog sartorius muscle during isometric, and isotonic contractions. *J. Muscle Res. Cell Motil.* 15:319–348.

Mejean, C., M. Boyer, J. P. Labbe, L. Marlier, Y. Benyamin, and C. Roustan. 1987. Anti-actin antibodies: an immunological approach to the myosin actin, and the tropomyosin interfaces. *Biochem. J.* 244:571–577.

Miller, L., M. Kalnoski, Z. Yunossi, J. C. Bulinski, and E. Reisler. 1987. Antibodies directed against N-terminal residues on actin do not block acto-myosin binding. *Biochemistry.* 26:6064–6070.

Mitsui, T., and H. Ohshima. 1993. An induced potential model for myosin head motion along an actin filament in contracting muscle. I. Fundamental muscle properties. *Mem. Inst. Sci. Technol. Meiji Univ.* 32: 31–62.

Moir, A. J. G., B. A. Levine, A. J. Goodearl, and I. P. Trayer. 1987. The interaction of actin with myosin subfragment-1, and with PPDM-crosslinked S1: a H-1-NMR investigation. *J. Muscle Res. Cell Motil.* 8:68–69.

Muller, C. W., and G. E. Schulz. 1992. Structure of the complex between adenylate kinase from escherichiacoli, and the inhibition for AP5A refined at 1.9 Å resolution: a model for a catalytic transition state. *J. Mol. Biol.* 224:159–177.

Pai, E. F., U. Krengel, G. A. Petsko, R. S. Goody, W. Kabsch, and A. Wittinghofer. 1990. Refined crystal-structure of the triphosphate conformation of H-ras P21 at 1.35 Å resolution: implications for the mechanism of GTP hydrolysis. *EMBO J.* 9:2351.

Piazzessi, G., and V. Lombardi. 1995. A cross-bridge model that is able to explain mechanical and energetic properties of shortening muscle. *Biophysical J.* 68:1966–1979.

Poole, K. J. V., K. C. Holmes, G. Evans, G. Rosenbaum, I. Rayment, and M. Lorenz. 1995. Control of actomyosin interaction. *Biophys. J.* 68: 348s.

Rayment, I., H. M. Holden, M. Whittaker, C. B. Yohn, M. Lorenz, K. C. Holmes, and R. A. Milligan. 1993a. Structure of the actin-myosin complex, and its implication for muscle contraction. *Science.* 261: 58–65.

Rayment, I., W. R. Rypnieswski, K. Schmidt-Bäse, R. Smith, D. R. Tomchick, M. M. Benning, D. A. Winkelman, G. Wesemberg, and H. M. Holden. 1993b. Three-dimensional structure of myosin subfragment-1: a molecular motor. *Science.* 261:50–58.

Reedy, M. K., K. C. Holmes, and R. T. Tregear. 1965. Induced changes in orientation of the cross-bridges of glycerinated insect flight muscle. *Nature.* 207:1276–1280.

Rogers, N. K., G. R. Moore, and M. J. E. Sternberg. 1985. Electrostatic infractions in globular-proteins: calculations of the pH dependence of the redox potential of cytochrome C551. *J. Mol. Biol.* 182:613–616.

Schroder, R. R., D. J. Manstein, W. Jahn, H. Holden, I. Rayment, K. C. Holmes, and A. Spudich. 1993. 3-dimensional atomic model of F-actin decorated with dictyostelium myosin-S1. *Nature.* 364:171–174.

Spudich, J. A. 1994. How molecular motors work. *Nature.* 372:515–518.

Sternberg, M. J. E., F. R. F. Hayes, A. J. Russell, P. G. Thomas, and A. R. Fersht. 1987. Prediction of electrostatic effects of engineering of protein changes. *Nature.* 330:86–88.

Sutoh, K., M. Ando, K. Sutoh, and Y. Y. Tyoshima. 1991. Site-directed mutations of *Dictyostelium* actin: disruption of a negative charge cluster at the N terminus. *Proc. Natl. Acad. Sci. USA.* 88:7711–7714.

Tong, L., A. M. de Vos, M. V. Milburn, and S. H. Kim. 1991. Crystal structures at 2.2 Å resolution of the catalytic domains of normal RAS protein, and an oncogenic mutant complexed with GDP. *J. Mol. Biol.* 217:503–516.

Van Eyk, J. E., and R. S. Hodges. 1991. A synthetic peptide of the N-terminus of actin interacts with myosin. *Biochemistry.* 30: 11676–11682.

Verlet, L. 1967. Computer "experiments" on classical fluids. I. Thermodynamical properties of Lennard-Jones molecules. *Physiol. Rev.* 159: 98–103.

Yamamoto, K. 1989. Binding manner of actin to the Lysine-rich sequence of myosin subfragment-1 in the presence, and absence of ATP. *Biochemistry.* 28:5573–5577.

Yount, G. Y., D. Lawson, and I. Rayment. 1995. Is myosin a "back door" enzyme? *Biophys. J.* 68:44s–49s.